


RESEARCH ARTICLE

10.1029/2018JE005756

Impact Ejecta and Gardening in the Lunar Polar Regions

J. R. Szalay¹ , P. Pokorný^{2,3,4} , Z. Sternovsky^{5,6,7} , Z. Kupihar⁸ , A. R. Poppe⁹ , and M. Horányi^{6,7,10} 

Key Points:

- Meteoroid bombardment provides a pathway to redistribute lunar regolith
- Meteoroid impacts into the lunar regolith may deposit more heat into the surface than impacts into hard, icy surfaces
- A polar orbiting dust detector would sample significant quantities of polar ejecta and potentially characterize lunar surface water content

Supporting Information:

- Supporting Information S1
- Table S1
- Table S2
- Table S3

Correspondence to:

J. R. Szalay,
jszalay@princeton.edu

Citation:

Szalay, J. R., Pokorný, P., Sternovsky, Z., Kupihar, Z., Poppe, A. R., & Horányi, M. (2019). Impact ejecta and gardening in the lunar polar regions. *Journal of Geophysical Research: Planets*, 124. <https://doi.org/10.1029/2018JE005756>

Received 10 JUL 2018

Accepted 28 NOV 2018

Accepted article online 3 DEC 2018

¹Department of Astrophysical Sciences, Princeton University, Princeton, NJ, USA, ²Heliophysics Science Division, GSFC/NASA, Greenbelt, MD, USA, ³Astrophysics Science Division, GSFC/NASA, Greenbelt, MD, USA, ⁴Department of Physics, Catholic University of America, Washington, DC, USA, ⁵Aerospace Engineering Sciences Department, University of Colorado Boulder, Boulder, CO, USA, ⁶Laboratory for Atmospheric and Space Physics, Boulder, CO, USA, ⁷Institute for Modeling Plasma, Atmospheres, and Cosmic Dust, Boulder, CO, USA, ⁸Department of Biochemistry, University of Colorado Boulder, Boulder, CO, USA, ⁹Space Sciences Laboratory, University of California, Berkeley, CA, USA, ¹⁰Department of Physics, University of Colorado Boulder, Boulder, CO, USA

Abstract The Moon is continually bombarded by interplanetary meteoroids. While many of the meteoroid sources are near the ecliptic plane, a significant population of high-inclination meteoroids exists at 1 au that bombards the lunar polar regions. Building on previous measurements of the response of the lunar impact ejecta cloud to known meteoroid sources, we develop an ejecta model for the entire lunar surface by incorporating the high-inclination sources. We find that the polar regions of the Moon experience similar quantities of impact ejecta production as the equator. Due to the enhanced impactor fluxes near the equator and at high latitudes on the dawn side, lunar regolith is preferentially distributed to the mid to high-latitude regions over long timescales, providing a pathway to mix regolith from different regions. We find impact ejecta yields at the Moon to be significantly lower than the Galilean moons, suggesting meteoroids deliver more energy to the local regolith and can be an important driver in the evolution of volatiles near the lunar surface. Additionally, we find that a polar orbiting spacecraft equipped with a dust analyzer can measure appreciable quantities of lunar ejecta near the poles to constrain the water content in the polar regions.

Plain Language Summary The Moon is continually impacted by small particles shed primarily from comets, which impact the Moon from a variety of organized directions. These impacts kick up a significant amount of the lunar soil above the lunar surface and sustain a permanently present cloud of ejecta around the Moon. Previous work categorized the ejecta cloud in the Moon's equatorial plane. Here we extend that work to understand the ejecta environment in the high-latitude polar regions of the Moon. We find that there are significant quantities of impact ejecta generated in the polar regions. Over long periods of time, lunar material is preferentially distributed to the mid to high-latitude regions, providing a pathway to mix equatorial and polar regolith. Additionally, we find that a polar orbiting spacecraft equipped with a dust analyzer can measure appreciable quantities of lunar ejecta near the poles to constrain the water content in the polar regions.

1. Introduction

Airless surfaces like the Moon's are completely exposed to interplanetary dust particles (IDPs) or meteoroid impacts. The lunar surface is covered with a layer of loose rocky material, including fine dust particles. This regolith has been formed and remains continually reworked by the intermittent impacts of comets and asteroids and the continual bombardment by meteoroids. Each meteoroid impact produces more ejecta mass compared to the primary impactor mass, most of which at the Moon remains bound and returns to reblanket the surface in a process known as impact gardening (Arnold, 1975; Gault et al., 1974; Morris, 1978; Pieters & Noble, 2016).

Impact gardening is an active process occurring on all airless bodies in the solar system and may also be an important driver in the evolution of water on the lunar surface. Water is thought to be continually delivered to the Moon through geological timescales by water-bearing comets and asteroids and produced continuously in situ by the impacts of solar wind protons of oxygen-rich minerals exposed on the surface (Arnold, 1979).

In addition to potentially delivering water over long timescales (e.g., Furi et al., 2012), high-speed meteoroid impacts can mobilize secondary ejecta dust particles, atoms, and molecules (Farrell et al., 2015; Hodges, 2002; Hurley et al., 2017, 2012). Additionally, the bound ejecta will continually rain back onto the lunar surface and may bury exposed volatiles over time. Other surface processes that can lead to mobilization, transport, and loss of water molecules and other volatiles include solar heating, photochemical processes, and solar wind sputtering. However, since these drivers are minimized at high latitudes, permanently shadowed regions (PSRs) are thought to be efficient volatile traps (Colaprete et al., 2010; Watson et al., 1961). Meteoroid impacts are an important driver governing the evolution of volatiles in these regions (Crider & Vondrak, 2003; Mandt et al., 2016). Hence, knowledge of the high-latitude meteoroid flux and subsequent burial rate of bound ejecta are important to understand the evolution of volatiles in the lunar polar regions.

The meteoroid environment at 1 au is composed of dust grains shed from comets and asteroids. A combination of size-dependent forces causes the ejected grains to decouple from their parent bodies and follow divergent trajectories over time. These grains comprise the “sporadic background,” which is highly anisotropic and typically organized into six sources: the helion/antihelion (HE/AH), the apex/anti-apex (AP/AA), and the northern/southern toroidal (NT/ST) sources (Campbell-Brown, 2008; Janches et al., 2000; Jones & Brown, 1993; Pokorný et al., 2014). Each of the sporadic sources has distinct parent body sources, which leads to different characteristic directionalities and impact velocities.

Impactor fluxes to lunar polar regions have been historically difficult to constrain, given the paucity of available data. However, recent Earth-based observational and modeling efforts have revealed a persistent, high-speed and high-inclination source of meteoroids at 1 au shed from Halley-type comets that continually bombard the lunar polar regions (Pokorný et al., 2014). Additionally, recent in situ ejecta measurements made at the Moon have enabled a detailed understanding of the structure of the impact-generated, permanently present lunar ejecta cloud and subsequent gardening rates near the lunar equatorial plane (Horányi et al., 2015; Szalay & Horányi, 2016a). Here we extend those equatorial measurements to the lunar polar regions by incorporating the high-latitude toroidal meteoroid sources to constrain the associated impact gardening rates. In section 2, we describe the impact ejecta data set and ejecta production model. Combining equatorial impact ejecta observations with a global model of the impact ejecta mass production at the lunar surface, we estimate the impact ejecta burial rate in section 3. In section 4, we apply similar analysis to predict the impact ejecta cloud structure at high latitudes and discuss the potential for constraining the water content in the polar regions from future measurements of this cloud in section 5. We conclude in section 6 with a discussion on the implications of these results.

2. Ejecta Model Description

In this section, we describe the impact ejecta model we use to estimate the lunar burial rates. First, we derive a model of all upgoing ejecta due to meteoroid bombardment by expanding the previous equatorial lunar ejecta model to the entire lunar surface. Next, we assume all upgoing ejecta is launched into a narrow 10° cone and track where this ejecta redistributes on the surface, integrating over the entire surface. Taking the difference of the upgoing ejecta and downgoing redistributed ejecta, we then calculate the net uncovering or burial rate.

Impact ejecta measurements at the Moon have been taken by the Lunar Dust Experiment (LDEX), an impact-ionization dust detector (Horányi et al., 2014) that flew aboard the *Lunar Atmosphere and Dust Environment Explorer* (LADEE) mission (Elphic et al., 2014) from October 2013 to April 2014. LADEE visited altitudes of a few to ~ 260 km and selenographic latitudes of -23° to $+24^\circ$. The LDEX instrument was capable of detecting grains with radii $a \geq 0.3 \mu\text{m}$ at the LADEE orbital speed of 1.6–1.7 km/s. LDEX measurements revealed a permanently present, asymmetric dust cloud engulfing the Moon (Horányi et al., 2015), with a large density enhancement on the lunar apex hemisphere (in the direction of orbital motion). These measurements also determined the size distribution, where the ejecta exhibited a consistent power law for particles as small as $a = 0.3 \mu\text{m}$. Following previous analyses (e.g., Szalay & Horányi, 2016a), we assume that the power law found by LDEX can be reasonably extended down to a grain size of $a_0 = 0.1 \mu\text{m}$, and hence, all gardening calculations utilize a lower limit of $a_0 = 0.1 \mu\text{m}$.

Previous analyses of the observed lunar impact ejecta cloud found that its structure was well matched by the response of the surface to sporadic sources in the equatorial plane (Szalay & Horányi, 2015a). Specifically, the HE/AH and AP sources (e.g., Campbell-Brown, 2008). A minor contribution from the AA source was later

included to account for the small ejecta densities near dusk (Szalay & Horányi, 2016a). In this study, we expand that fit to include the high-latitude NT/ST sources (Pokorný et al., 2014). Each source is modeled as a collimated beam from a specific radiant direction, and the subsequent impact ejecta response is assumed to follow

$$M^+ \propto F_m m^\alpha v^\beta \cos^2 \varphi, \quad (1)$$

where m is the characteristic mass of the impactors, F_m is the mass flux, v is the impactor speed, $\alpha = 0.23$ and $\beta = 2.46$ are experimentally determined constants, and φ is the angle of impact ejecta relative to the surface normal (Gault et al., 1974; Koschny & Grün, 2001a; Szalay & Horányi, 2015a). Equation (1) is given as a proportionality relation since M^+ is scaled to the actual lunar values derived by LDEX measurements, described below. Following the previous empirical fit to the lunar dust cloud (Szalay & Horányi, 2016a), where M^+ is directly proportional to the density of ejecta at the surface. The density n (m^{-3}) as a function of altitude h (km), local time ϕ , latitude λ , and particle radius a_μ (μm) is then given by

$$n(h, \phi, \lambda, a) = e^{-h/h_0} a_\mu^{-q} n_w \sum_s w_s \cos^3(\Delta\varphi_s) \Theta(|\Delta\varphi_s| - \pi/2), \quad (2)$$

where $h_0 = 200$ km, $q = 2.7$ (Horányi et al., 2015), n_w is a normalization density (m^{-3}) that is scaled to be consistent with LDEX measurements, s is the index for the sources, w_s is the relative weight of each source where $\sum_s w_s = 1$, $\Delta\varphi_s = \cos^{-1}[\cos \phi \cos \phi_s + \sin \phi \sin \phi_s \cos(\lambda - \lambda_s)]$ is the angle to a given source, and Θ is the Heaviside function. The additional $\cos \varphi$ in the $\cos^3 \varphi$ is from the surface area projection of the flux. Here we use Solar-Selenocentric-Ecliptic coordinates. Based on previous analyses (Szalay & Horányi, 2015a, 2016a), the AP/AA sources are centered at $\phi_{AP} = 6$ LT and $\phi_{AA} = 18$ LT. The HE/AH sources are offset from the apex direction at $\phi_{HE} = 10.3$ LT and $\phi_{AH} = 1.7$ LT. All four of these sources reside in the $\lambda = 0^\circ$ plane. Previously, relative weights were determined to be $w_{HE} = w_{AH} = 0.24$, $w_{AP} = 0.49$, and $w_{AA} = 0.03$ from comparison to LDEX data (Szalay & Horányi, 2016a).

Here we introduce the NT and ST sources, centered at $\phi = 6$ LT (dawn) and offset by angle $\lambda_{NT} = -\lambda_{ST}$ in latitude. For simplicity, we set $\lambda_{NT} = 60^\circ$ based on the approximate center of the dawn feature (Pokorný et al., 2014); however, we will test our results to the sensitivity of this assumption. To determine the relative weight of w_s for the NT/ST sources, we make further simplifying approximations. First, we assume that the NT/ST sources have the same characteristic mass as the HE/AH source, thereby allowing us to ignore the mass dependence in equation (1). Without loss of generality, we compare the weights of the HE and NT source. The ratio of these two sources is then given by

$$r = \frac{w_{NT}}{w_{HE}} = \frac{F_{NT} \langle v_{NT} \rangle_\beta}{F_{HE} \langle v_{HE} \rangle_\beta}, \quad (3)$$

where

$$\langle v \rangle_\beta = \left(\frac{\int_0^\infty f(v) v^\beta dv}{\int_0^\infty f(v) dv} \right)^{1/\beta}, \quad (4)$$

is the characteristic speed corresponding to the β moment of the speed distribution function. Using previous models of the speed distribution for the HE (Nesvorný, Janches, et al., 2011) and NT (Pokorný et al., 2014) sources at Earth, we determine the speed distribution at the Moon by unfocusing the Earth-based distributions to infinity then focusing it to the surface of the Moon, following existing focusing relations (Colombo et al., 1966; Spahn et al., 2006). For $\beta = 2.46$, we find $\langle v_{HE} \rangle_\beta = 13$ km/s and $\langle v_{NT} \rangle_\beta = 30$ km/s at the Moon and for the flux ratio, we use $F_{NT}/F_{HE} = 0.2$ to 0.4 (Campbell-Brown & Jones, 2006). This leads to $w_{NT} = 0.5 w_{HE}$ to $0.9 w_{HE}$ with an average value of $0.7 w_{HE}$. With the inclusion of the NT/ST dawnside sources, they will contribute to the equatorial dust density near dawn. Therefore, to maintain a good match with the measured equatorial ejecta cloud structure, we reduce the total contribution of the AP source, where a reduction by 25% was found to maintain reasonable consistency. The new weights are now $w_{HE} = w_{AH} = 0.198$, $w_{AP} = 0.303$, $w_{AA} = 0.025$, and $w_{NT} = w_{ST} = 0.138$, and in this new setup, $n_w = 4.7 \times 10^{-4} \text{ m}^{-3}$.

Figure 1a shows the impact ejecta density at the surface, $n_0(\phi, \lambda) = n(h = 0, \phi, \lambda, a = 0.3 \mu\text{m})$, where the top row shows each source separately to illustrate the differences in each source's ejecta production. While we calculate gardening quantities in the following section for $a \geq 0.1 \mu\text{m}$, here we show n_0 for $a \geq 0.3 \mu\text{m}$ in order to directly compare with the existing LDEX measurements taken with this threshold. Note that all maps

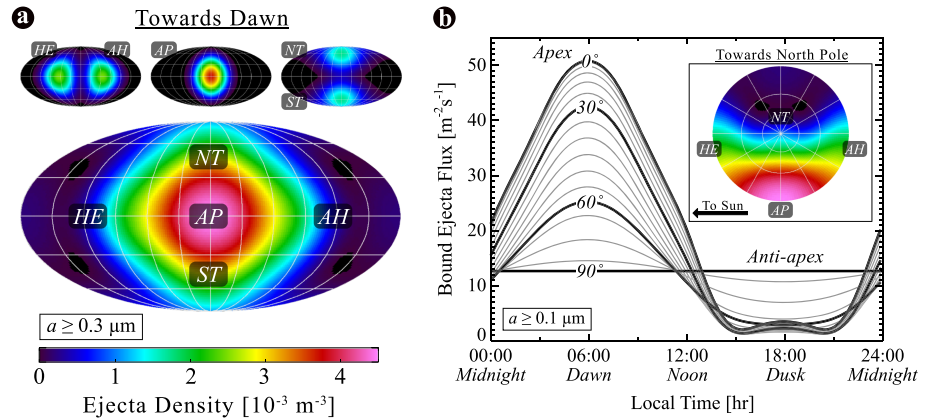


Figure 1. (a) Ejecta density n_0 at the surface in a Mollweide projection for the various sources individually (above) and combined (below) in a “windshield” view looking from the center of the Moon outward. Latitude/longitude lines are shown every 30° . (b) Total upgoing ejecta flux as a function of LT over all latitudes. The inset shows polar stereographic projection of n_0 in the northern hemisphere, also in the same windshield view as (a), but with a viewpoint looking north. HE = helion; AH = antihelion; AP = apex; NT = northern toroidal; ST = southern toroidal.

in Figure 1 are shown in a “windshield” view from the vantage point of an observer sitting in the center of the Moon looking outward. This is chosen to be consistent with the large majority of meteor radiant maps shown in the literature. For Figure 1a, this viewpoint is centered on the apex direction, or direction of the Moon’s orbital motion about the Sun. For Figure 1b, the viewpoint is from an observer in the center of the Moon, facing the apex direction and looking up toward the north pole.

3. Estimating the High-Latitude Gardening Rate

The surface density is directly proportional to the bound upgoing ejecta flux

$$F_{av}(\lambda) = \langle n_0(\phi, \lambda) \rangle_\phi \bar{v}, \quad (5)$$

where $\bar{v} = \int_0^{v_{esc}} v f(v) dv \approx 660 \text{ m/s}$ is the average ejecta speed, $v_{esc} = 2.4 \text{ km/s}$ is the lunar escape speed, and $\langle n_0(\phi, \lambda) \rangle_\phi$ is the local time averaged surface density. Here F_{av} represent the average upgoing flux from a patch on the lunar surface near the equator over a lunar day. This number is a derived result from the LDEX measurements at the Moon and is a direct consequence from converting impact rates observed at LADEE’s altitude to the upgoing ejecta flux at the surface necessary to reproduce these measurements. Previous empirical models of the lunar ejecta cloud provide an analytic estimate for the total bound surface flux as a function of angle from apex in the lunar equatorial plane (Szalay & Horányi, 2016a). At the equator, $F_{av}(\lambda = 0^\circ) = 24 \pm 13 \text{ m}^{-2} \cdot \text{s}^{-1}$ for $a \geq 0.1 \mu\text{m}$. The error is calculated following previous analyses, by incorporating a 20% error from assuming all grains are at their turning points and an average 35% error from the fitted and observed values of the lunar ejecta density.

We scale the model output yield map such that its longitude averaged value at the equator is $F_{av}(\lambda = 0^\circ) = 24 \text{ m}^{-2} \cdot \text{s}^{-1}$ to create a surface bound ejecta flux map, scaling the ejecta densities in Figure 1a. Figure 1b shows the surface bound upgoing ejecta flux as a function of LT individually for every 5° latitude. As an implicit assumption of our model, the northern and southern fluxes are identical. As shown in this figure, near the equator the bound ejecta flux is highly pronounced in the apex direction, due to the large characteristic speed of the apex source meteoroids and their efficiency in generating large quantities of impact ejecta. For increasing latitudes, this asymmetry is less apparent, as the apex source is not able to access high-latitude terrain and the toroidal sources become more prominent. As implicitly assumed, the toroidal mass production peaks at $(\phi = 6 \text{ LT}, \lambda = 60^\circ)$. With such a high-latitude meteoroid flux, the toroidals are able to access a portion of the anti-apex hemisphere, similar to Mercury’s impactor environment (Pokorny et al., 2018) and lead to the more symmetric high-latitude ejecta flux profiles shown in Figure 1b. Very high latitudes experience nearly constant bound ejecta fluxes of $\sim 10 \text{ m}^{-2} \cdot \text{s}^{-1}$.

To determine how the soil redistributes due to impacts, we convolve the response of a single plume with the upgoing ejecta flux predicted from the model to determine the net flux. Previous analyses for the LDEX

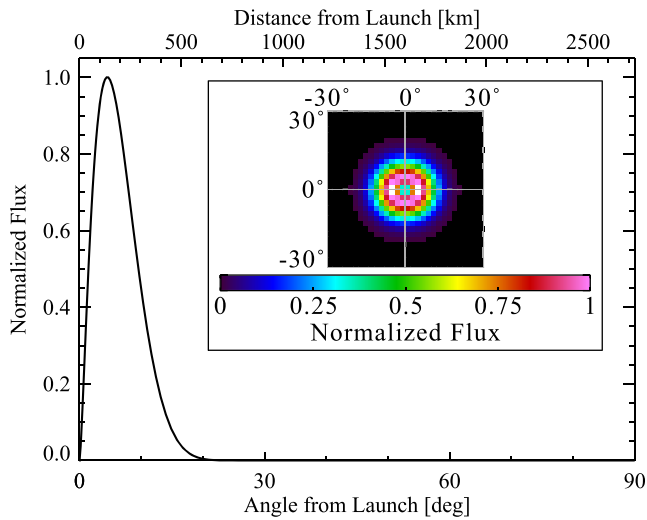


Figure 2. Normalized flux distribution of impact ejecta for a single plume at the equator with a 10° cone angle.

data set calculated gardening rates assuming all grains were launched with no horizontal velocity component (Szalay & Horányi, 2016a). This allows for the calculation of how much material is excavated and overturned over a given time span, but it is not possible to determine soil redistribution from a purely vertical motion framework. Here we relax that assumption. Analysis of LDEX observations of dense ejecta plumes indicates the high-speed impact ejecta may be distributed into a narrow cone with an opening angle of approximately 10° from surface normal (Bernardoni et al., 2018). For simplicity, we assume all impacts create a symmetric impact ejecta plume. We model a single ejecta plume and track where its material accumulated. In this simple setup, we simulated the ejection of grains with a uniform angular distribution and a speed distribution of

$$f(\hat{v}) = \frac{\eta \hat{v}}{(1 - \hat{v}^2)^2} e^{-\frac{\beta \hat{v}^2}{1 - \hat{v}^2}}, \quad (6)$$

where $\hat{v} = v/v_{\text{esc}}$, $\beta = 8.69$, and $\eta = 7.2 \times 10^{-3}$ s/m (Szalay & Horányi, 2016a). Only grains with initial speeds less than lunar escape speed are tracked.

This speed distribution is derived from the high-altitude (>1 km) LDEX measurements and accounts for the high-speed, narrow angle component of impact ejecta. As LADEE did not transit lower than 1 km for an appreciable amount of time, LDEX was not able to characterize or observe any slower ejecta populations that might exist with initial ejection speeds less than approximately 60 m/s, the minimum initial ejection speed needed to reach 1-km altitude at the Moon. The shape of the derived speed distribution in equation (6) has a monotonically decreasing flux of ejecta for decreasing speeds below ~600 m/s and suggests a very small amount of ejecta exists below 60 m/s should the speed distribution trend hold to near-zero ejection speeds. The ejecta modeled here is then the high-speed component able to reach kilometer-scale altitudes, and there may be an additional population of slow-speed and/or high-angle ejecta not captured by the LDEX measurements.

We emphasize that the LDEX measurements cannot conclusively determine if there is an additional population of low-speed ejecta below 60 m/s. Were such a population were to exist, this slow-speed ejecta could contribute to the near-impact cratering blanket and to very local gardening near the impact. The impactors generating the ejecta measured by LDEX are most likely small, submillimeter impactors at very high speeds in the range a few up to ~60 km/s. These impacts are excavating material from the very top portion of the lunar regolith, which is highly porous in the top few millimeters to centimeters (Hapke & Sato, 2016; Ohtake et al., 2010). Near-crater ejecta blankets from impacts into porous materials can be suppressed under certain conditions (Housen et al., 2018); however, experiments under the exact impactor and target properties considered here have not been performed to our knowledge. The exact structure of impact craters in such a regime remains to be quantitatively constrained and would warrant additional laboratory investigations. As such, we do not consider the effects of any possible low-speed ejecta populations and model the ejecta population directly measured by LDEX. Additionally, if a population of low-speed ejecta exists for the ejecta plumes investigated in this study, it would not effectively redistribute material over large distances since its ejection speeds would be so low.

Note that we do not account for secondary ejecta production from meteoroid bombardment. The ejecta considered in this work is generated by impacts of meteoroids with average speeds of tens of kilometers per second. For example, average impact speeds for the HE and NT sources are $\langle v_{HE} \rangle_1 = 11$ km/s and $\langle v_{NT} \rangle_1 = 29$ km/s, respectively. The subsequent ejecta that reimpacts the lunar surface is bound and must have “reimpact” speeds smaller than the lunar escape speed of 2.4 km/s. There are significantly less particles with large ejection speeds near escape, as equation (6) has an average ejection speed of ~0.7 km/s and gives ~15% of bound ejecta with speeds over 1 km/s. Even the small portion of higher speed ejecta, for example, the 15% from 1 to 2.4 km/s, have significantly lower impactor speeds than tens of kilometers per second of the primary meteoroids sustaining the lunar ejecta cloud. Since impact ejecta production scales steeply with the impactor speed, $\propto v^{2.46}$ as given in equation (1), secondary impactors are not able to generate appreciable amounts of high-speed secondary ejecta considered in this work compared to the primary meteoroids at tens of kilometers per second.

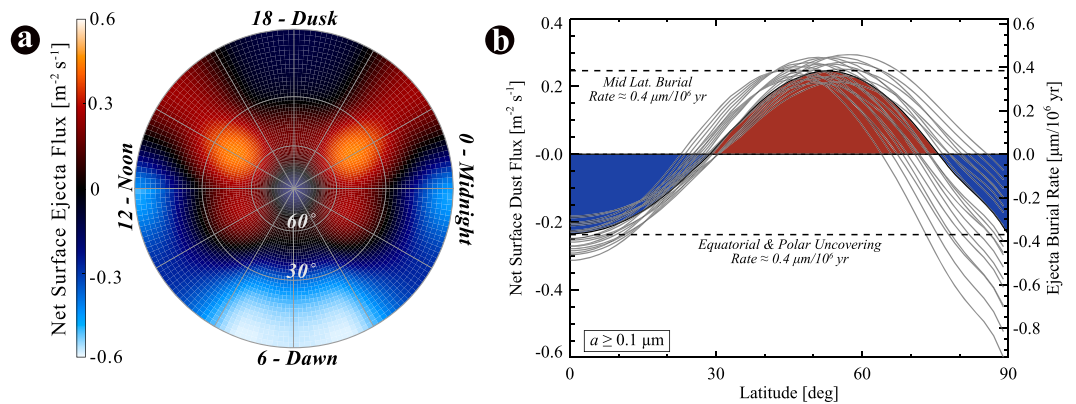


Figure 3. (a) Burial rate in the northern hemisphere in a stereographic projection. (b) Local-time-averaged burial rate as a function of latitude. Gray lines indicate the burial rates over a variation of toroidal parameters ($\lambda_{NT} = 55^\circ$ to 70° and $F_{NT}/F_{HE} = 0.2$ to 0.4). Over long timescales, material is lost from the equatorial region and redistributed towards the mid to high latitudes. High-latitudes $>75^\circ$ also lose material towards lower latitudes due to the toroidal impactors.

Figure 2 shows the results of this single plume simulation, where the bulk of ejecta material accumulates in a ring around 100–200 km from the ejecta plume center and is a consequence of the average ejecta speed of ~ 0.7 km/s. Note that this ejecta redistribution profile is calculated for the high-speed ejecta measured by LDEX and does not consider any slow-speed near-impact ejecta that may be produced by the impact. As previously discussed, the exact quantity of slow-speed ejecta for small, high-speed impactors into the porous upper lunar regolith remains to be determined and warrants additional study. We can convolve the response of a single plume (the downgoing flux) with the upgoing ejecta flux predicted from the model to determine the net flux.

The characteristic cross-sectional area for this flux is calculated by integrating over the size distribution function, $\sigma = \int_{a_0}^{a_{\max}} f(a)\pi a^2 da \approx 0.13 \mu\text{m}^2$, where the approximation has been made for $a_{\max} \gg a_0$ following previous analyses (Szalay & Horányi, 2016a). The accumulation timescale, after which the surface will be entirely covered by a single layer of impact ejecta is $\tau = 1/F\sigma$ with a characteristic thickness of $d \approx \sqrt{\sigma} = 0.37 \mu\text{m}$. Hence, the burial rate, the rate at which a flat plate on the surface would accumulate bound impact ejecta, is $\delta = d/\tau = F\sigma^{3/2}$.

Figure 3a shows the burial rate in a stereographic projection looking toward the north pole from the center of the Moon. Since the AP source is the dominant impact ejecta producer, it excavates and redistributes the most material at the Moon, as evidenced by the large net loss of ejecta in the equator centered on 6 LT (dawn). The toroidal sources, also centered at dawn, but at $\pm 60^\circ$ latitude, excavate and redistribute material away from the toroidal radiant. The combination of all impactor sources, which are concentrated on the dawn hemisphere with the exception of the weak anti-apex source, leads to the majority of dawnside lunar surface to be in a net negative flux (loss) state, redistributing itself to the duskside. Figure 3b shows the LT-averaged burial rate as a function of latitude. Since impact ejecta has a higher production rate in the equatorial region due to the retrograde, high-speed AP impactors, as well as the prograde HE/AH impactors, material is preferentially redistributed towards higher latitude regions over long timescales. We find that within $\sim 30^\circ$ of the equator, the depth of the lunar regolith is very slowly decreasing, which is redistributed to higher latitudes. The high-latitude toroidal sources serve to excavate polar material and redistribute it toward lower latitudes such that above $\sim 75^\circ$ latitude, the polar regions are also in a net loss due to IDP bombardment. This provides a pathway to redistribute material from different regions of the lunar surface over long timescales.

To constrain the error of our results, we varied ϕ_{NT} from 55° to 70° in increments of 5° and the ratio $r = w_{NT}/w_{HE}$ (equation (3)) from 0.5 to 0.9 in increments of 0.1, corresponding to $F_{NT}/F_{HE} = 0.2$ to 0.4 . The gray lines in Figure 3 show the results for this range of parameters. The curves in our parameter study predict a similar trend as the nominal assumption, with equatorial uncovering rates in the range of 0.2 – $0.3 \mu\text{m}$ per 10^6 years and mid-latitude burial rates of up to $0.4 \mu\text{m}$ per 10^6 years ($\tau = 10^6$ years for a single layer of burial). Strengthening and raising the latitude of the toroidal sources would also lead to larger losses in the polar regions, as indicated by the gray curves which fall below the nominal case in the polar regions.

Additionally, with a model for the ejecta production over the entire surface, we can revisit estimates of the total ejecta mass of the lunar dust cloud (Horányi et al., 2015). The average ejecta flux over the entire surface is $16 \text{ m}^{-2} \cdot \text{s}^{-1}$ (for $a \geq 0.1 \text{ }\mu\text{m}$). Assuming the ejecta size distribution follows a power law (cumulative size index of 2.7) between $0.1 \text{ }\mu\text{m}$ and 1 mm , and a bulk density of 2.5 g/cm^3 , the average mass for a single ejecta particle is $1.4 \times 10^{-15} \text{ kg}$ ($0.5\text{-}\mu\text{m}$ radius). Integrating over the entire surface, the Moon produces $\sim 18 \text{ t/day}$ of high-speed ejecta. The average lifetime of grains is given by $T = \int t(v)f(v)dv = 17 \text{ min}$, where $t(v)$ is the ballistic lifetime from launch to reimpact of surface ejecta accounting for the radially varying gravitational force. The total ejecta mass is 210 kg , given by the product of average mass flux and lifetime and about a factor of two higher than previous initial estimates of 120 kg (Horányi et al., 2015).

Scaling the total meteoroid influx at Earth of 43 t/day (Carrillo-Sánchez et al., 2016) to the Moon's cross-sectional area, we would expect a few tons per day of meteoroid material to bombard the lunar surface. Our observed ejecta production rate of 18 t/day suggests that the mass yield of meteoroids producing high-speed ejecta is on the order of 10, which is substantially lower than that for the icy Galilean satellites (Krüger et al., 2003), which had estimated yields of 10^3 to 10^4 , 2 to 3 orders of magnitude higher than that observed here. This discrepancy could be due to a number of reasons.

If a large fraction of the impact ejecta is launched from the surface at low speeds, LDEX would not have measured such a population. LDEX visited down to altitudes of a few kilometers and observed a consistent exponential scaling of the density. LDEX could not observe dust particles ejected from the surface at less than $50\text{--}100 \text{ m/s}$, so it is possible there is an enhancement of low-speed impact ejecta that was never observed by LADEE. If the lunar surface yield is similar to the icy Galilean satellites, this would imply that $< 1\%$ of the total impact ejecta reaches altitudes greater than 1 km .

Another possibility is that the dusty, regolith surface of the Moon does not respond to meteoroid bombardment in the same manner as hard, icy surfaces. While the canonical yield experiment was performed for different mixtures of ice and silicate content (Koschny & Grün, 2001b), all targets were shot into an icy solid surface from which the ejecta yield was estimated. Impacts of small meteoroids ($\sim 100 \text{ }\mu\text{m}$) into the Moon's regolith surface may not eject as much material as a hard surface, as discussed in recent work (e.g., Costello et al., 2018), and previously modeled (Anders et al., 2012). The ejecta observed by LDEX may have been launched from the surface under an entirely different regime of impact ejecta physics, where a much larger fraction of the energy is available to be partitioned into local heating of the regolith instead of into the kinetic energy of launched particles. If this is the case, small meteoroids may be highly efficient at depositing their energy into the lunar regolith and may therefore be even more important in governing the evolution of ice in the polar regions (e.g., Farrell et al., 2013) than previously thought.

4. Ejecta Measurements for Polar Orbiting Spacecraft

Impact ejecta, in addition to modifying surface features over time by continually raining back onto the surface, carries key information about the surface composition. A spacecraft equipped with an impact-ionization dust detector with chemical analysis capability would be able to map the compositional features of the ejecta to their surface origins with a resolution of the altitude of the spacecraft. Here we discuss measurements that could be made with an orbiting spacecraft. We employ a canonical orbit of 100-km altitude with an orbital speed of 1.6 km/s , which gives a detection threshold for an LDEX-type instrument of $0.3 \text{ }\mu\text{m}$ (Horányi et al., 2014). Using equation (2), we can estimate the structure of the high-latitude lunar impact ejecta cloud. We do not expect significant quantities of electrostatically lofted dust to be present at high altitudes as previous in situ efforts did not detect this population (Szalay & Horányi, 2015b); hence, we only model the contribution of impact ejecta to the overall dust density.

Figure 4a shows side views of the predicted impact ejecta cloud in three separate polar orbits: from 6 to 18, 9 to 21, and 12 to 0 LT, along with the location of the 100-km orbit. The size of the ejecta cloud/orbit is not to scale with the Moon. The bottom row of Figure 4 shows density and impact rate profiles for the three LT slices in black as a function of latitude, where the beginning of the orbit is at the south pole. Impact rates are calculated as if LDEX were transiting these locations, with 70-cm^2 effective area (Horányi et al., 2014). The polar orbits all have very similar average densities and subsequent average impact rates (about 1 min^{-1}) compared to LADEE's equatorial orbit.

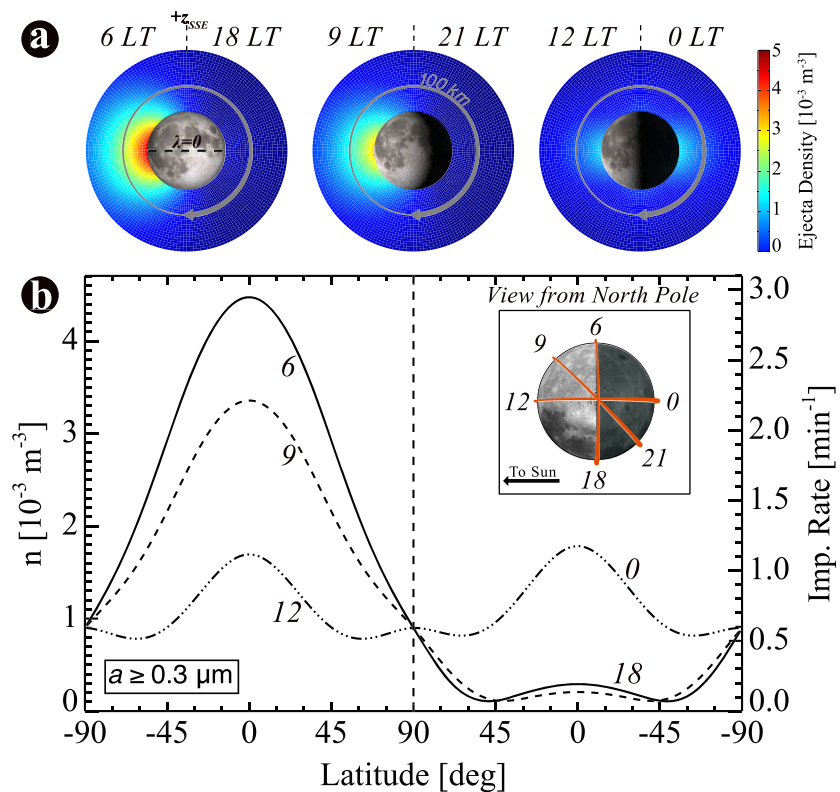


Figure 4. (a) Side view of the lunar dust densities for three planes perpendicular to the $+z$ axis, up to 250-km altitude (not to scale). The location of the 100-km orbit is shown on each. (b) Local dust density and impact rate for an orbiting spacecraft as a function of latitude. The inset shows the three orbits in a view from the top. All quantities shown for $a \geq 0.3 \mu\text{m}$. Lunar image credit: NASA/Bill Dunford.

5. Detectability of Water in Impact Ejecta Spectra

With such large impact rates near the polar regions and PSRs, which may contain enhanced surface water content (e.g., Li & Milliken, 2017), we investigate the possibility of identifying water on particles originating from the lunar surface. In this section, we discuss a potential mechanism that would allow detection of water on dust grains impacting an orbiting dust analyzer. With such a capability, impact ejecta measurements near the lunar polar regions would not only constrain meteoroid bombardment in the polar regions but would also potentially be able to characterize the water cycle at the Moon.

Dust analyzer instruments are capable of measuring time-of-flight (TOF) mass spectra from impact ionized dust particles (e.g., Srama et al., 2005; Sternovsky et al., 2007, 2015). Laboratory experiments showed the relation between the measured mass spectra and the elemental composition of the dust particles, potentially allowing identification of mineralogical information from in situ TOF spectra (e.g., Fiege et al., 2014). At

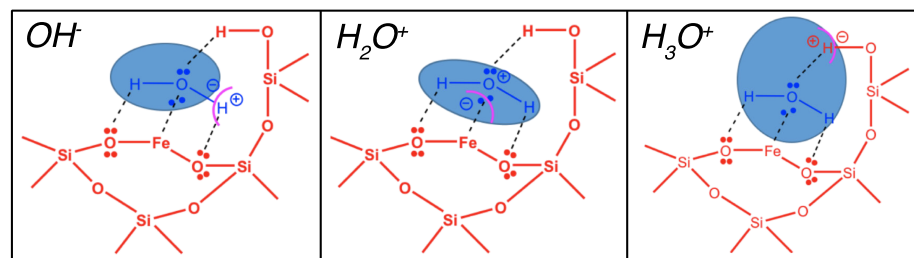


Figure 5. Possible cleavages of the ionization of a water molecule assisted by the surface, and generating OH^- , H_2O^+ , and H_3O^+ ions. Dashed lines show the electrostatic interactions between the surface and the water molecules, and the pink arc indicates where the cleavage occurred.

low-impact speeds, typically below 3–5 km/s, mass spectra are dominated by easy-to-ionize species (e.g., Na, K, or Ca), while elements from the bulk composition with higher ionization energies (e.g., C, O, and Si) only appear at higher impact velocities.

A recent experiment studied the impact ionization of olivine and magnesite dust samples over a wide impact speed range of about 3–30 km/s (Hillier et al., 2018). One surprising outcome of this study is that water features are present in the spectra even at the lowest impact speeds studied. Water/hydroxyl species (O, OH, H₂O, and H₃O) are present in cation spectra for both samples, although more pronounced for magnesite. Similarly, anion spectra also exhibit O and OH features. While this study was limited to impact speeds ≥ 3 km/s, the data for magnesite suggest that water features may very well be observable at even lower impact speeds, that is, down to typical lunar spacecraft orbit speeds of ~ 1.6 km/s.

The ionization energy of a water molecule in a gas phase is 12.4 eV and ~ 9.5 eV in the condensed phase (Novakovskaya, 2007). This value, however, is still high for the ionization of water molecules from the bulk of the dust particles. Recent analysis suggests ionized water signatures in spectra at low velocities are likely to originate from the surface, where OH groups and/or physisorbed water molecules are abundant (Hillier et al., 2018). The surface can act like a catalyst, decreasing the energy barrier needed to break a bond within the water molecule. These bonds are weakened through electrostatic interactions (H-bond, dipole-dipole force) with the surface. Upon desorption after a dust particle impact, the surface may retain an ionic particle from the water molecule (e.g., H⁺ or e⁻), generating a water/hydroxyl ion. Figure 5 illustrates three scenarios for the energy from a dust impact to result into cleavages generating OH⁻, H₂O⁺, and H₃O⁺ ions on a hypothesized surface. Lucking et al. (2015) performed molecular dynamics theoretical calculations of the oxidation of water on a TiO₂ surface. In this more complex, yet analogous case, the presence of the polar surface can reduce the energy needed for ionizing water molecules down to 1.2 eV. The lunar regolith is known to have an active surface, such that the atomic network on the interface contains active sites where strong electrostatic interaction with polarizable molecules will occur. The surface of the lunar regolith can act as a highly active heterogeneous catalyst containing both acidic and basic sites. Such a catalyst then can lower the effective energy for ionizing water molecules, leading to detectable water spectra in impact measurements near the polar regions. Since water features may manifest either as positive or negative ions, it would be best to perform TOF analysis of polar ejecta for both polarities.

Recent efforts have been undertaken to constrain water content on the lunar surface by using data sets from multiple spacecraft observations (e.g., Fisher et al., 2017; Hendrix et al., 2012; Li & Milliken, 2017; Li et al., 2018; Sim et al., 2017; Wöhler et al., 2017). These studies have indicated the water distribution on the lunar surface varies as a function of latitude, degree of space weathering, maria versus highland terrain, and local time, yet many mysteries still exist regarding the lunar water cycle. If impact ejecta are able to retain a chemical imprint of the water content from its source region, in situ dust analyzer measurements of lunar ejecta could be critical in understanding the water cycle at the Moon in a complementary manner to remote observations.

6. Discussion and Conclusions

In this work, we find the toroidal sources (i.e., high-inclination meteoroids from Halley-type comets) are responsible for producing significant quantities of impact ejecta in the lunar polar regions. Meteoroids from these sources should also liberate large quantities of neutral species (e.g., Colaprete et al., 2016; Hurley et al., 2017; Szalay et al., 2016). Due to the enhanced impact ejecta production near the lunar equator and around 60° on the dawnside, equatorial material can migrate to the mid to high-latitudes over long timescales. While lunar polar wander was constrained by meter-depth water features that persisted over the last approximately billion years (Siegler et al., 2016), which is consistent with the low values of polar burial rates of $< 1 \mu\text{m}/10^6$ years derived here, impact bombardment may contaminate the top layer of regolith in the mid to high-latitude regions. Secondary ejecta is not considered due to the low reimpact speeds of ejecta compared to the high-speed primary meteoroids sustaining the lunar impact ejecta environment at high altitudes. Additionally, while the net transport is from the equator and polar regions to the mid-latitudes, there will be some mixing of both polar and equatorial regions due to bombardment. Material from the polar regions may be excavated by the toroidal sources and redistributed to the equatorial regions as previously suggested (Farrell et al., 2013).

The impactor sizes considered here are typically much smaller than those that generate observable craters. LDEX may be measuring impact ejecta from primary impactors at largest up to ~ 30 g (Szalay et al., 2018),

notably during meteoroid showers such as the Geminids. Large sporadic impactors >30 g, such as those detected by the Lunar Impact Monitoring Program (Suggs et al., 2008), are not expected to be observed due to their low flux. For example, flux estimates of sporadic impactors >30 g are $6 \times 10^{-4} \text{ km}^{-2} \cdot \text{year}^{-1}$ (Suggs et al., 2014). Assuming LDEX can detect an impact that occurs within an area on the surface equal to its altitude squared, it is able to detect impacts within $A = 2,500 \text{ km}^2$ for an average altitude of 50 km. LDEX operated with total operating time of 80 cumulative days and would have needed to double that total detection time to detect just a single ejecta plume from a sporadic impactor >30 g. Additionally, larger impactors (e.g., Speyerer et al., 2016) may generate more ejecta per event but are most likely confined to more equatorial orbits. While estimates from LDEX may serve as a lower limit near the equatorial plane, at high latitudes the total burial/uncovering rate may be closer to those estimated here.

Accounting for the impact ejecta production over the entire surface, the total quantity of ejecta produced is surprisingly low compared to our expectations from impact ejecta measurements at the icy Galilean moons. One explanation for this could be that the Moon's fluffy regolith surface is not able to produce as much impact ejecta compared to a hard, icy surface. If this is the case, the impact energy of incident meteoroids to the surface could be partitioned more into local heating of the regolith than into the kinetic energy of ballistic ejecta. Such a finding suggests meteoroids may play a more important role in governing the evolution of ice in the polar regions than previously thought.

All results derived in this work utilized a model for impact ejecta generation, summing six separate sources represented by $\cos^3 \varphi$ functions. Corrections to the model using a dynamical interplanetary dust particle impactor model (e.g., Janches et al., 2018; Nesvorný, Janches, et al., 2011; Nesvorný, Vokrouhlický, et al., 2011; Pokorný et al., 2014, 2017) could potentially improve ejecta estimates. For example, the toroidal source is more of a ring-like flux structure (e.g., Pokorný et al., 2014) than a collimated beam at 60° latitude as assumed here. A more spread out flux distribution will lead to a different overall burial rate profile; however, we do not expect the estimates given in this paper to be modified by more than a factor of a few, given the sensitivity test discussed in section 3. Additionally, we assumed the sources were symmetrically distributed in Solar-Selenocentric-Ecliptic coordinates and static in time. However, the impactor distribution is not perfectly symmetric and there are synodic and annual variations, as previously observed by LDEX (Szalay & Horányi, 2015a) and recently modeled (Janches et al., 2018). Additionally, we assume that the various sources all have similar mass distributions, however, modest changes in the expected M^+ maps may be expected for relaxing this assumption. The speed dependence used here follows an existing laboratory calibration for impacts into icy-silicate mixtures (Koschny & Grün, 2001a) and does not necessarily capture all the relevant physics involved in meteoroid-regolith impacts. While changes to the speed dependence for the lunar ejecta production could modify the structure of the predicted ejecta cloud, we do not anticipate a large discrepancy from the results presented in this paper as we have already constrained the equatorial ejecta cloud with LDEX measurements.

We also find that a polar orbiting spacecraft can detect similar average impact rates compared to the equatorial LADEE orbit. During several of the known meteoroid showers, LDEX measured localized dust density enhancements, many of which allowed full or partial reconstruction of the shower radiants (Szalay & Horányi, 2016b). During the Geminids, LDEX observations revealed fine structure in this shower in a manner unique to dust detector data (Szalay et al., 2018). Were a polar orbiting spacecraft to make impact ejecta measurements during a meteoroid shower, for example, the Quadrantids in a similar orbit to the 6 to 18 LT one included here, these measurements may similarly uncover additional substructures in high-latitude meteoroid streams. Additionally, preliminary data from the laboratory and theoretical considerations suggest that water molecules adsorbed on the lunar regolith may get ionized and liberated to gas phase at the orbital speed of a spacecraft. We presented a mechanism that would allow detection of surficial water on grains and suggest laboratory results are needed to further quantify the amount of detectable water in lunar ejecta. Modern dust impact analyzers are capable of identifying increased water content in ejecta particles originating from more water-rich regions and can provide critical constraints on the water cycle at the Moon.

Acknowledgments

Data for figures not directly derived from equation (2) are included as supporting information. J. R. S. was supported by NASA's Lunar Data Analysis Program (LDAP), Grant 80NSSC17K0702. M. H. was supported by the Institute for Modeling Plasma, Atmospheres, and Cosmic Dust of NASA's Solar System Exploration Research Virtual Institute. A. R. P. was supported by the DREAM2 team of NASA's SSERVI Institute, grant NNX14AG16A.

References

- Anders, C., Bringa, E. M., Fioretti, F. D., Ziegenhain, G., & Urbassek, H. M. (2012). Crater formation caused by nanoparticle impact: A molecular dynamics study of crater volume and shape. *Physical Review B*, *85*(23), 326–14.
- Arnold, J. R. (1975). A Monte Carlo model for the gardening of the lunar regolith. *The Moon*, *13*(1-3), 159–172.
- Arnold, J. R. (1979). Ice in the lunar polar regions. *Journal of Geophysical Research*, *84*(B10), 5659–5668.
- Bernardoni, E. A., Szalay, J. R., & Horányi, M. (2018). Impact ejecta plumes at the Moon. *Geophysical Research Letters*, *45*. <https://doi.org/10.1029/2018GL079994>

- Campbell-Brown, M. D. (2008). High resolution radiant distribution and orbits of sporadic radar meteoroids. *Icarus*, *196*, 144–163. <https://doi.org/10.1016/j.icarus.2008.02.022>
- Campbell-Brown, M., & Jones, J. (2006). Annual variation of sporadic radar meteor rates. *Monthly Notices of the Royal Astronomical Society*, *367*(2), 709–716.
- Carrillo-Sánchez, J. D., Nesvorný, D., Pokorný, P., Janches, D., & Plane, J. M. C. (2016). Sources of cosmic dust in the Earth's atmosphere. *Geophysical Research Letters*, *43*, 11. <https://doi.org/10.1002/2016GL071697>
- Colaprete, A., Sarantos, M., Wooden, D. H., Stubbs, T. J., Cook, A. M., & Shirley, M. (2016). How surface composition and meteoroid impacts mediate sodium and potassium in the lunar exosphere. *Science*, *351*(6270), 249–252.
- Colaprete, A., Schultz, P., Heldmann, J., Wooden, D., Shirley, M., Ennico, K., et al. (2010). Detection of water in the LCROSS ejecta plume. *Science*, *330*, 463–468. <https://doi.org/10.1126/science.1186986>
- Colombo, G., Lautman, D. A., & Shapiro, I. I. (1966). The Earth's dust belt: Fact or fiction? 2. Gravitational focusing and Jacobi capture. *Journal of Geophysical Research*, *71*, 5705–5717.
- Costello, E. S., Ghent, R. R., & Lucey, P. G. (2018). The mixing of lunar regolith: Vital updates to a canonical model. *Icarus*, *314*, 327–344.
- Crider, D. H., & Vondrak, R. R. (2003). Space weathering effects on lunar cold trap deposits. *Journal of Geophysical Research*, *108*(E), 5079. <https://doi.org/10.1029/2002JE002030>
- Elphic, R. C., Delory, G. T., Hine, B. P., Mahaffy, P., Horanyi, M., Colaprete, A., et al. (2014). The Lunar Atmosphere and Dust Environment Explorer mission. *Space Science Reviews*, *185*, 3–25.
- Farrell, W. M., Hurley, D. M., Hodges, R. R., Killen, R. M., Halekas, J. S., Zimmerman, M. I., & Delory, G. T. (2013). Redistribution of lunar polar water to mid-latitudes and its role in forming an OH veneer. *Planetary and Space Science*, *89*(C), 15–20.
- Farrell, W. M., Hurley, D. M., & Zimmerman, M. I. (2015). Spillage of lunar polar crater volatiles onto adjacent terrains: The case for dynamic processes. *Geophysical Research Letters*, *42*, 3160–3165. <https://doi.org/10.1002/2015GL063200>
- Fiege, K., Trieloff, M., Hillier, J. K., Guglielmino, M., Postberg, F., Srama, R., et al. (2014). Calibration of relative sensitivity factors for impact ionization detectors with high-velocity silicate microparticles. *Icarus*, *241*, 336–345. <https://doi.org/10.1016/j.icarus.2014.07.015>
- Fisher, E. A., Lucey, P. G., Lemelin, M., Greenhagen, B. T., Siegler, M. A., Mazarico, E., et al. (2017). Evidence for surface water ice in the lunar polar regions using reflectance measurements from the Lunar Orbiter Laser Altimeter and temperature measurements from the Diviner Lunar Radiometer Experiment. *Icarus*, *292*, 74–85. <https://doi.org/10.1016/j.icarus.2017.03.023>
- Füri, E., Marty, B., & Asponov, S. S. (2012). Constraints on the flux of meteoritic and cometary water on the Moon from volatile element (N-Ar) analyses of single lunar soil grains, Luna 24 core. *Icarus*, *218*(1), 220–229.
- Gault, D. E., Hoerz, F., Brownlee, D. E., & Hartung, J. B. (1974). Mixing of the lunar regolith. In *Proceedings of the 5th Lunar and Planetary Science Conference* (Vol. 3, pp. 2365–2386). New York: Pergamon Press.
- Hapke, B., & Sato, H. (2016). The porosity of the upper lunar regolith. *Icarus*, *273*(C), 75–83.
- Hendrix, A. R., Retherford, K. D., Randall Gladstone, G., Hurley, D. M., Feldman, P. D., Egan, A. F., et al. (2012). The lunar far-UV albedo: Indicator of hydration and weathering. *Journal of Geophysical Research*, *117*, E12001. <https://doi.org/10.1029/2012JE004252>
- Hillier, J. K., Sternovsky, Z., Kempf, S., Trieloff, M., Guglielmino, M., Postberg, F., & Price, M. (2018). Impact ionisation mass spectrometry of platinum-coated olivine and magnesite-dominated cosmic dust analogues. *Planetary and Space Science*, *156*, 96–110. <https://doi.org/10.1016/j.pss.2017.10.002>
- Hodges, R. R. (2002). Ice in the lunar polar regions revisited. *Journal of Geophysical Research*, *107*(E2), 5011–7.
- Horányi, M., Sternovsky, Z., Lankton, M., Dumont, C., Gagnard, S., Gathright, D., et al. (2014). The Lunar Dust Experiment (LDEX) onboard the Lunar Atmosphere and Dust Environment Explorer (LADEE) mission. *Space Science Reviews*, *185*, 93–113. https://doi.org/10.1007/978-3-319-18717-4_5
- Horányi, M., Szalay, J. R., Kempf, S., Schmidt, J., Grün, E., Srama, R., & Sternovsky, Z. (2015). A permanent, asymmetric dust cloud around the Moon. *Nature*, *522*(7556). <https://doi.org/10.1038/nature14479>
- Housen, K. R., Sweet, W. J., & Holsapple, K. A. (2018). Impacts into porous asteroids. *Icarus*, *300*, 72–96.
- Hurley, D. M., Cook, J. C., Retherford, K. D., Greathouse, T., Gladstone, G. R., Mandt, K., et al. (2017). Contributions of solar wind and micrometeoroids to molecular hydrogen in the lunar exosphere. *Icarus*, *283*(C), 31–37.
- Hurley, D. M., Lawrence, D. J., Bussey, D. B. J., Vondrak, R. R., Elphic, R. C., & Gladstone, G. R. (2012). Two-dimensional distribution of volatiles in the lunar regolith from space weathering simulations. *Geophysical Research Letters*, *39*, L09203. <https://doi.org/10.1029/2012GL051105>
- Janches, D., Mathews, J. D., Meisel, D. D., Getman, V. S., & Zhou, Q. H. (2000). Doppler studies of near-antapex UHF radar micrometeors. *Icarus*, *143*(2), 347–353.
- Janches, D., Pokorný, P., Sarantos, M., Szalay, J. R., Horányi, M., & Nesvorný, D. (2018). Constraining the ratio of micrometeoroids from Short and Long Period Comets at 1 AU from LADEE observations of the Lunar Dust Cloud. *Geophysical Research Letters*, *45*, 1713–1722. <https://doi.org/10.1002/2017GL076065>
- Jones, J., & Brown, P. (1993). Sporadic meteor radiant distributions—Orbital survey results. *Monthly Notices of the Royal Astronomical Society*, *265*, 524.
- Koschny, D., & Grün, E. (2001a). Impacts into ice-silicate mixtures: Crater morphologies, volumes, depth-to-diameter ratios, and yield. *Icarus*, *154*, 391–401. <https://doi.org/10.1006/icar.2001.6707>
- Koschny, D., & Grün, E. (2001b). Impacts into ice-silicate mixtures: Ejecta mass and size distributions. *Icarus*, *154*, 402–411. <https://doi.org/10.1006/icar.2001.6708>
- Krüger, H., Krivov, A. V., Sremčević, M., & Grün, E. (2003). Impact-generated dust clouds surrounding the Galilean moons. *Icarus*, *164*(1), 170–187.
- Li, S., Lucey, P. G., Milliken, R. E., Hayne, P. O., Fisher, E., Williams, J.-P., et al. (2018). Direct evidence of surface exposed water ice in the lunar polar regions. *Proceedings of the National Academy of Science*, *115*, 8907–8912. <https://doi.org/10.1073/pnas.1802345115>
- Li, S., & Milliken, R. E. (2017). Water on the surface of the Moon as seen by the Moon Mineralogy Mapper: Distribution, abundance, and origins. *Science Advances*, *3*(9), e1701471.
- Lucking, M., Sun, Y.-Y., West, D., & Zhang, S. (2015). A nucleus-coupled electron transfer mechanism for TiO₂-catalyzed water splitting. *Physical Chemistry Chemical Physics*, *17*(26), 16,779–16,783.
- Mandt, K. E., Greathouse, T. K., Retherford, K. D., Gladstone, G. R., Jordan, A. P., Lemelin, M., et al. (2016). LRO-LAMP detection of geologically young craters within lunar permanently shaded regions. *Icarus*, *273*(C), 114–120.
- Morris, R. V. (1978). In situ reworking (gardening) of the lunar surface—Evidence from the Apollo cores. *Lunar and Planetary Science Conference*, *9*, 1801–1811.
- Nesvorný, D., Janches, D., Vokrouhlický, D., Pokorný, P., Bottke, W. F., & Jenniskens, P. (2011). Dynamical model for the zodiacal cloud and sporadic meteors. *The Astrophysical Journal*, *743*(2), 129.

- Nesvorný, D., Vokrouhlický, D., Pokorný, P., & Janches, D. (2011). Dynamics of dust particles released from OORT cloud comets and their contribution to radar meteors. *The Astrophysical Journal*, *743*(1), 37–12.
- Novakovskaya, Y. V. (2007). Theoretical estimation of the ionization potential of water in condensed phase. ii. superficial water layers. *Protection of Metals*, *43*(1), 22–33.
- Ohtake, M., Matsunaga, T., Yokota, Y., Yamamoto, S., Ogawa, Y., Morota, T., et al. (2010). Deriving the absolute reflectance of lunar surface using SELENE (Kaguya) multiband imager data. *Space Science Reviews*, *154*(1-4), 57–77.
- Pieters, C. M., & Noble, S. K. (2016). Space weathering on airless bodies. *Journal of Geophysical Research: Planets*, *121*, 1865–1884. <https://doi.org/10.1002/2016JE005128>
- Pokorný, P., Sarantos, M., & Janches, D. (2017). Reconciling the dawn-dusk asymmetry in Mercury's exosphere with the micrometeoroid impact directionality. *The Astrophysical Journal Letters*, *842*, L17. <https://doi.org/10.3847/2041-8213/aa775d>
- Pokorný, P., Sarantos, M., & Janches, D. (2018). A comprehensive model of the meteoroid environment around Mercury. *The Astrophysical Journal*, *863*(1), 31. <https://doi.org/10.3847/1538-4357/aad051>
- Pokorný, P., Vokrouhlický, D., Nesvorný, D., Campbell-Brown, M., & Brown, P. (2014). Dynamical model for the toroidal sporadic meteors. *The Astrophysical Journal*, *789*(1), 25.
- Siegler, M., Miller, R. S., Keane, J. T., Laneuville, M., Paige, D. A., Matsuyama, I., et al. (2016). Lunar true polar wander inferred from polar hydrogen. *Nature*, *531*(7), 480–484.
- Sim, C. K., Kim, S. S., Lucey, P. G., Garrick-Bethell, I., & Choi, Y.-J. (2017). Asymmetric space weathering on lunar crater walls. *Geophysical Research Letters*, *44*, 11,273–11,281. <https://doi.org/10.1002/2017GL075338>
- Spahn, F., Schmidt, J., Albers, N., Hörning, M., Makuch, M., Seif, M., et al. (2006). Cassini dust measurements at enceladus and implications for the origin of the E ring. *Science*, *311*, 1416–1418. <https://doi.org/10.1126/science.1121375>
- Speyerer, E. J., Povilaitis, R. Z., Robinson, M. S., & Wagner, R. V. (2016). Quantifying crater production and regolith overturn on the Moon with temporal imaging. *Nature Publishing Group*, *538*(7624), 215–218.
- Srama, R., Srowig, A., Rachev, M., Grün, E., Kempf, S., Moragas-Klostermeyer, G., et al. (2005). Development of an advanced dust telescope. In *Modern Meteor Science An Interdisciplinary View* (pp. 211–220). Dordrecht: Springer.
- Sternovsky, Z., Amyx, K., Bano, G., Landgraf, M., Horányi, M., Knappmiller, S., et al. (2007). Large area mass analyzer instrument for the chemical analysis of interstellar dust particles. *Review of Scientific Instruments*, *78*(1), 14501. <https://doi.org/10.1063/1.2431089>
- Sternovsky, Z., Gerner, A., Grün, E., Horányi, M., Kempf, S., Maute, K., et al. (2015). Hyperdust: An advanced in-situ detection and chemical analysis of microparticles in space. In *2015 IEEE Aerospace Conference*, Big Sky, MT, USA, pp. 1–10.
- Suggs, R. M., Cooke, W. J., Suggs, R. J., Swift, W. R., & Hollon, N. (2008). The NASA lunar impact monitoring program. *Earth*, *102*(1), 293–298.
- Suggs, R. M., Moser, D. E., Cooke, W. J., & Suggs, R. J. (2014). The flux of kilogram-sized meteoroids from lunar impact monitoring. *Icarus*, *238*, 23–36. <https://doi.org/10.1016/j.icarus.2014.04.032>
- Szalay, J. R., & Horányi, M. (2015a). Annual variation and synodic modulation of the sporadic meteoroid flux to the moon. *Geophysical Research Letters*, *42*, 10,580–10,584. <https://doi.org/10.1002/2015GL066908>
- Szalay, J. R., & Horányi, M. (2015b). The search for electrostatically lofted grains above the Moon with the lunar dust experiment. *Geophysical Research Letters*, *42*, 5141–5146. <https://doi.org/10.1002/2015GL064324>
- Szalay, J. R., & Horányi, M. (2016a). Lunar meteoritic gardening rate derived from in situ LADEE/LDEX measurements. *Geophysical Research Letters*, *43*, 4893–4898. <https://doi.org/10.1002/2016GL069148>
- Szalay, J. R., & Horányi, M. (2016b). Detecting meteoroid streams with an in-situ dust detector above an airless body. *Icarus*, *275*, 221–231. <https://doi.org/10.1016/j.icarus.2016.04.024>
- Szalay, J. R., Horányi, M., Colaprete, A., & Sarantos, M. (2016). Meteoritic influence on sodium and potassium abundance in the lunar exosphere measured by LADEE. *Geophysical Research Letters*, *43*, 6096–6102. <https://doi.org/10.1002/2016GL069541>
- Szalay, J. R., Pokorný, P., Jenniskens, P., & Horányi, M. (2018). Activity of the 2013 Geminid meteoroid stream at the Moon. *Monthly Notices of the Royal Astronomical Society*, *474*(3), 4225–4231. <https://doi.org/10.1093/mnras/stx3007>
- Watson, K., Murray, B., & Brown, H. (1961). On the possible presence of ice on the Moon. *Journal of Geophysical Research*, *66*, 1598–1600. <https://doi.org/10.1029/JZ066i005p01598>
- Wöhler, C., Grumpe, A., Berezhnoy, A. A., & Shevchenko, V. V. (2017). Time-of-day-global distribution of lunar surficial water/hydroxyl. *Science Advances*, *3*(9), e1701286.